

Intraplanar Magnetic Excitations in $\text{Na}_{\frac{1}{2}}\text{CoO}_2$: An Inelastic Neutron Study

J. Wooldridge^{1,*}, G. Balakrishnan¹, D. McK. Paul¹, C. Frost², P. Bourges³, and M. R. Lees¹

¹*Department of Physics, University of Warwick, Coventry, CV4 7AL, UK*

²*ISIS, Rutherford Appleton Laboratory, ChilTERN, Didcot, OX11 0QZ, UK and*

³*Laboratoire Léon Brillouin (CEA-CNRS) CEA-Saclay, 91191 Gif-sur-Yvette Cedex, FRANCE*

(Dated: September 17, 2018)

Inelastic neutron scattering measurements mapping the in-plane magnetic interactions of $\text{Na}_{\frac{1}{2}}\text{CoO}_2$ reveal dispersive excitations at points above an energy gap $E_g = 11.5(5)$ meV at the superstructural Bragg reflections. The excitations are highly damped, broadening with increasing energy, and disappear at $\hbar\omega \approx 35$ meV, a strong indication that the magnetism is itinerant. Tilting into the *ac* plane reduces the value of E_g by 25%, suggesting that the dispersion along *c* is significant and the magnetic correlations are three-dimensional, as seen at the higher doping levels.

PACS numbers: 61.12.-q, 61.12.Ex, 67.57.Lm, 71.27.+a, 75.30.Fv, 72.10.Di

The discovery of superconductivity in hydrated sodium cobaltate in 2003¹ has generated a large volume of study in a relatively short space of time. The anhydrous parent phase is interesting in its own right; the system, at $x \geq 0.65$, is a Curie-Weiss metal with magnetic ordering below 22 K and the signature of magnetism, assigned to a spin density wave (SDW), depends sensitively on the level of sodium doping via its influence on the Co valence state. Recent neutron investigations of the SDW phase^{2,3} demonstrated that the magnetic ordering can be ascribed to an A-type antiferromagnetic (A-AFM) structure. In this system, however, only $1 - x$ of the Co sites carry spin, so that the simple Hamiltonian used to describe the excitation modes would only be valid if phase segregation into magnetic and nonmagnetic regions is assumed. This raises the question of whether the system really can be characterised by a model with localised spin ordering or whether an itinerant model with small charge disproportionation is more appropriate. A new regime emerges at $x = \frac{1}{2}$, with different magnetic ordering. At $T_M = 88$ K, long-ranged static AFM ordering occurs which has been clearly identified in neutron diffraction experiments⁴. At $T_{MI} = 53$ K, the material undergoes a metal to insulator transition (MIT). Further to this, there exists long-ranged ordering of the Na cations⁵ into quasi-onedimensional chains along *a*, enabling the crystal structure to be reclassified into an orthorhombic supercell of dimensions $(2a \times \sqrt{3}a \times c)$. In this crystal setting, there are now two Co sites. This led to speculation that the above transitions were the results of charge ordering (CO) in the CoO_2 planes, probably due to the influence of charge modulations in the Na layer. More recently, however, the notion of a charge ordered Mott-like transition has been disputed. NMR measurements⁶ did not deduce any large difference in charge state between the two sites. Crystal structure determination by powder neutron diffraction⁷ also failed to find a significant difference

between the Co-O hybridization on the two sites. A clear picture of the role of spin and orbital ordering in $\text{Na}_{\frac{1}{2}}\text{CoO}_2$ has yet to be defined. Here we present the first measurements of inelastic neutron scattering on this system to probe the nature of the interactions in the *ab* planes. A dispersive mode, magnetic in origin, is observed; the high damping and large velocity of the excitation indicates the possibility that the AFM ground state is itinerant. Preliminary investigations indicate that the system is also highly dispersive along *c*.

The samples were prepared by the floating zone method as described previously⁸. To confirm the stoichiometry of each sample, given that the magnetic transitions at T_{MI} and T_M occur only at $x = \frac{1}{2}$, magnetic susceptibility (χ) measurements were carried out in a Quantum Design MPMS-5S superconducting quantum interference device (SQUID) magnetometer on a range of samples; those selected for the experiments below had χ similar to previously reported measurements^{4,5,6}. The results indicated the sample was free from magnetic impurities (CoO or Co_3O_4). The heat capacity (C) measurements were carried out by a two-tau relaxation method in a Quantum Design PPMS. Inelastic neutron scattering measurements were taken on the MAPS spectrometer at ISIS (RAL) and the triple axis spectrometer (TAS) 2T1 at the Laboratoire Léon Brillouin (LLB) (CEA-CNRS). A mosaic of six crystals, each of mass ~ 0.5 g, was used for the experiment at ISIS. The samples were loaded into a CCR and cooled to 10 K. An incident neutron energy of 100 meV was selected and long counting times (typically 48 hours) were adopted to build up sufficient statistics in (\mathbf{Q}, E) space over the range of interest. Just one of these crystals was selected for the triple axis measurement in order to reduce the overall mosaic spread and optimise resolution. The crystal was cooled to 2.8 K in an orange cryostat with the *c* axis aligned vertically so that the Co moments were in the scattering plane.

Magnetic susceptibility and heat capacity measurements are shown in figure 1. Both the magnetic ordering and the metal-insulator transitions are clearly visible as

*Electronic address: J.Wooldridge@warwick.ac.uk

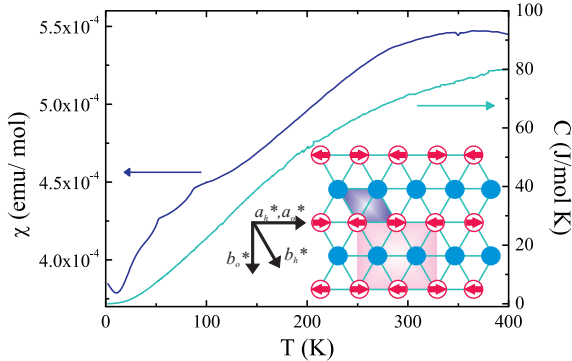


FIG. 1: Magnetic susceptibility ($H_{ab} = 5$ T) and heat capacity of $\text{Na}_{\frac{1}{2}}\text{CoO}_2$. The two transitions at T_M and T_{MI} are clearly visible in the magnetisation. On the contrary, the heat capacity data is featureless. The magnetic structure, first proposed by Choy et al.⁹ is presented in the inset, both the hexagonal (shaded blue) and orthorhombic (pink) unit cells are shown.

shoulders in the magnetisation. It is interesting to note that χ does not exhibit the Curie-Weiss-like character as seen in the SDW material: there is no signature of charge locality from the macroscopic measurements. The magnetic structure as measured by Gašparović et al.⁴ is presented in the inset. The symmetry breaking imposed by the orthorhombic supercell produces two separate Co sites, one of which is magnetically ordered ($\text{Co}^{4+} S=\frac{1}{2}$) and the other nonmagnetic ($\text{Co}^{3+} S=0$). In terms of the new unit cell, the system can be thought of as a simple G-type antiferromagnet with a magnetic propagation vector of $(1\frac{1}{2}1)$. The dynamics of the magnetism may be more complicated than suggested by this localised moment ordering picture; fluctuations on the nonordered rows of Co may affect the spin wave dispersion. The fact that the MIT occurs 35 K below T_M would suggest the transport carriers reside mainly on the second Co site. The opening of a gap on the part of the Fermi surface (FS) related to band containing these carriers would readily explain the onset of the insulating transition.

In order to confirm the nature of the magnetic ordering proposed by Gašparović et al.⁴ the crystals were first rotated by 30° to the incoming neutron beam in order to mimic the experimental setup as used by Boothroyd et al.¹⁰, where in-plane ferromagnetic (FM) ordering for an $x = 0.7$ crystal was visible as scattering around the origin, corresponding to a zero 2D magnetic ordering vector. No such scattering exists at this sodium level confirming the absence of FM coupling. The crystal was then rotated back to have $k_i \parallel c$. Inelastic scattering intensity is clearly visible (figure 2) at points above $(\frac{1}{2}00)$ in the parent hexagonal lattice. All six structural Bragg peaks are also visible in the elastic channel, which is at odds with a true long-ranged orthorhombic superstructure, where there should only be two. However, the integrated intensity of pairs of peaks diametrically opposite each other match, suggesting that the crystals exhibit twinning (rather tripling) in the basal plane and are not

just aligned along different equivalent direction choices of (100) . $S(\mathbf{Q}, \hbar\omega)$ maps were produced by slicing the data across different energy transfer levels. The small size of the sample resulted in a low signal to background ratio; the background itself is a product of multiple and instrumental scattering and increases with $|\mathbf{Q}|$. The energy resolution is dependent on the opening time of chopper used to monochromate the beam; this was relaxed to collect good statistics but ensured that elastic scattering extended up to 10 meV. As a result the background obscures the magnetic scattering at $|\mathbf{Q}| \geq 0.75$. Magnetic excitations should be visible as a cone of scattered intensity above the magnetic zone centre. There are no in-plane magnetic Bragg reflections⁴ and so, to further investigate the origin of the scattering seen here, measurements were completed at the TAS 2T1 at LLB.

At a temperature of 2.8 K, a clear peak is identifiable in both the inelastic and elastic channels (a non-magnetic superstructural peak resulting from Na ordering⁵) at $\mathbf{Q}=(\frac{1}{2}00)$. In order to access high enough energy transfers to examine the dispersion, it was necessary to move to the next Brillouin zone. The magnitude of the change in intensity between the two sites is comparable to that expected from the decrease in the magnetic form factor of Co^{4+} with the increase in $|\mathbf{Q}|$. A further indication that the signal is a result of 3D magnetic ordering is that the peak is destroyed by increasing the temperature to $\sim 2T_M$ (figure 3). Similar sets of \mathbf{Q} -scans were made at increasing energy transfers and are shown in figure 4. The excitation is gapped, with no scattered intensity visi-

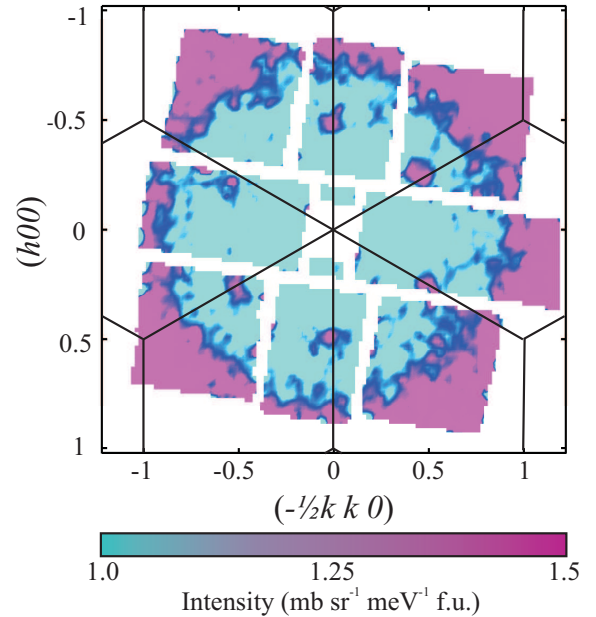


FIG. 2: Inelastic scattering in the $(hk0)$ plane summed over energy transfers of 10-20 meV. Scattering is visible at points corresponding to $[(100)](\frac{1}{2}00)$ in the [orthorhombic]hexagonal [super-]cell, although twinning reproduces the hexagonal symmetry. An overlay of the hexagonal reciprocal lattice is shown.

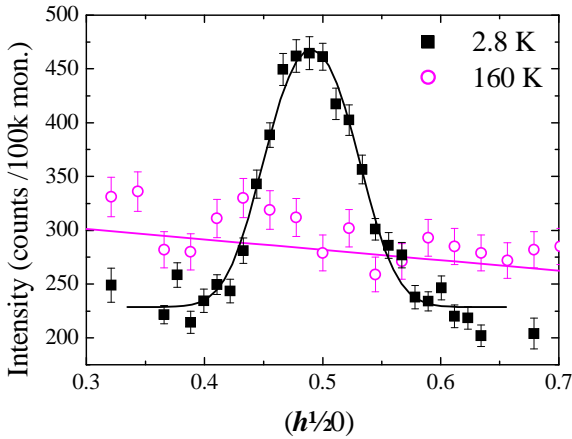


FIG. 3: Constant energy scans through $(\frac{1}{2}\frac{1}{2}0)$ at $\hbar\omega = 15$ meV. The superstructural Bragg peak at this \mathbf{Q} , and therefore the Na ordering, persists to high temperatures, whilst magnetic Bragg peaks at $(\frac{1}{2}\frac{1}{2}l_{odd})$ disappear at T_M ⁴. The inelastic signal has disappeared at twice the ordering temperature T_M , with an increased background corresponding to an enhancement of the incoherent and multi-phonon scattering.

ble below ~ 11.5 meV. The peaks are also overly damped, increasing in width with energy, whilst the overall dispersion is very steep. The data can be fitted to a linear dispersion $\hbar\omega = \sqrt{\Delta^2 + (D\mathbf{Q})^2}$ where Δ is the value of the energy gap and D the spin wave stiffness constant, more commonly referred to as the spin wave velocity in AFM systems. A fit to the data gives $\Delta = 11.5(5)$ meV and $D = 510(20)$ meV Å and is plotted as the solid line in panel B of figure 4.

To examine the excitation gap further, scans at constant \mathbf{Q} were made with increasing energy transfer. The gap was observed at both $(\frac{1}{2}00)$ and $(\frac{1}{2}\frac{1}{2}0)$ (figure 5) at $E_g = 11.5$ meV. The onset of scattering is sharp, and decays with increasing $\hbar\omega$. As seen at the higher doping levels, there exists an optical phonon (OP) at ~ 20 meV which dominates the signal in the Q-scans at that $\hbar\omega$. Since OP modes are relatively flat, it was possible to pick up the signal from the magnetic excitation once more at higher $\hbar\omega$. In order to correct for the additional phonon component to the scattering, another energy scan was taken at an offset position from the excitation at $(0.594 0.4 0)$, the exact values of $(hk0)$ being chosen to set the analyzer at the same 2θ position as the previous scan. The difference curve then removes the incoherent[phonon] scattering below[above] the gap. Finally, the sample was tilted slightly into the $(100)-(001)$ scattering plane and the same energy scan repeated for $\mathbf{Q}=(\frac{1}{2}0\frac{1}{2})$ (not shown). The value of E_g is shifted to ~ 9 meV suggesting that the dispersion along c is significant, a feature in accord with the 3D magnetic correlations reported for $x > 0.7$ ¹¹. $\mathbf{Q} = (\frac{1}{2}\frac{1}{2}0)$ is not a magnetic zone centre, no magnetic scattering exists at this point. In order to determine whether the excitation includes a spin wave gap, information of the dispersion along c is necessary.

These data exhibit features that are common to itinerant magnetic systems such as Cr^{12} or $\text{Mn}_3\text{Si}^{13}$, in which the highly damped dispersion, at the position of a magnetic Bragg peak, is seen to vary linearly in \mathbf{Q} up to energies of $\sim 2 k_B T_N$ and then rise vertically in a “chimney” of scattering. The dispersion here, however, remains linear in \mathbf{Q} until the signal disappears at $\sim 4 k_B T_N$. The most obvious method for determining the proportion of localised to itinerant spins in a FM material is to calculate the ratio of the high temperature paramagnetic moment and the low temperature saturated moment, equal to one in completely localised magnetic systems and greater than one for itinerant materials. This method is not applicable here; χ is not Curie-Weiss-like and the material has AFM ordering. For a localised spin system, the energy of the excitation at the zone boundary should be of the order of $k_B T_M$. An extrapolation of the data collected in this study predicts these two energies to be different by an order of magnitude. If the system exhibits low dimensionality, the energy scale characterising the excitation will relate to the strength of interactions along the spin chains, thus underestimating $k_B T_M$. However the loss of the excitation into a broadened continuum of decay modes, as witnessed here, indicates strongly that

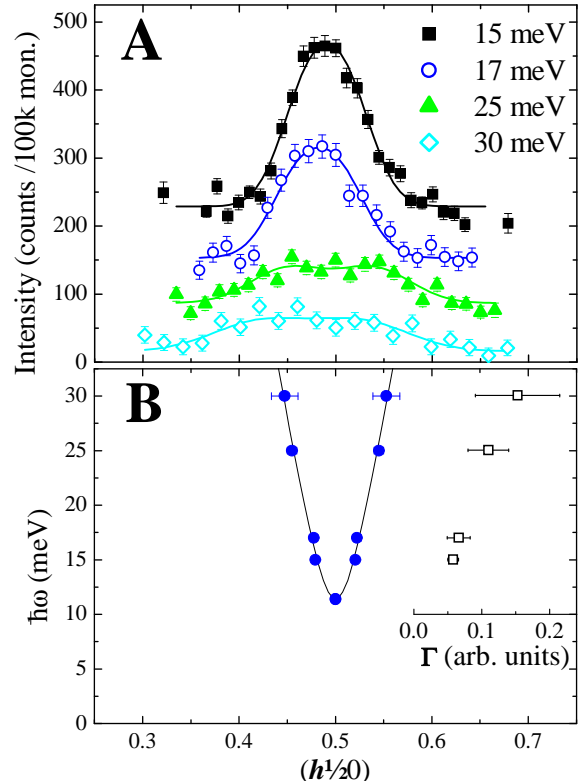


FIG. 4: A: Constant energy transfer scans at $\mathbf{Q}=(\frac{1}{2}\frac{1}{2}0)$ taken along (100) at 2.8 K. The datasets have been offset by -150 , -200 and -250 counts respectively for increasing energy transfer cuts. B: The measured spin wave dispersion along $(h\frac{1}{2}0)$ (the variation of the spin wave damping Γ with energy is shown in the inset); the excitation appears at ~ 11.5 meV.

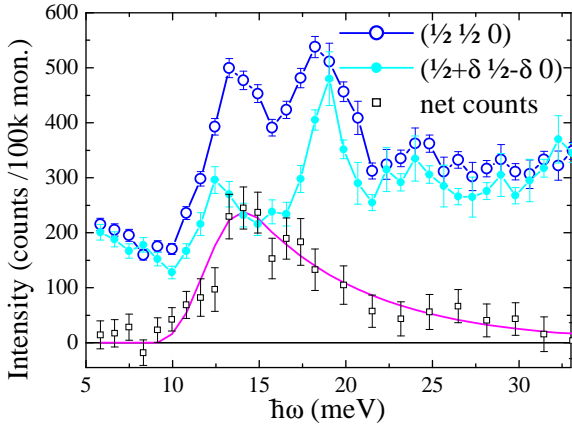


FIG. 5: Energy scans at $(\frac{1}{2} \frac{1}{2} 0)$. A background was taken at a position of $(\frac{1}{2} + \delta \frac{1}{2} - \delta 0)$ where $\delta \sim 0.1$ was chosen so that the spectrometer was aligned with the same 2θ positions as the on-peak measurements. The subtracted data (black open squares) is plotted; the line corresponds to the convolution of the experimental resolution ellipsoid and the intensity expected for an ideal gapped system ($E_g = 11.5$ meV).

the material is itinerant in character.

In the light of these results, the previously proposed model of a charge ordered ground state should be reconsidered. No evidence of either the T_M or T_{MI} transition can be seen in the specific heat. Recent NMR studies⁶ have suggested that both transitions could be attributed to spin density waves i.e. FS nesting effects, in which case T_{MI} would involve only modest modifications to the spin order, producing little measurable magnetic entropy. Alternatively, as mentioned above, the magnetism in $\text{Na}_{\frac{1}{2}}\text{CoO}_2$ may exhibit low dimensionality; in-plane correlations build slowly with decreasing temperature before locking in-phase along c at T_M . The phase diagram of sodium cobaltate is characterised by the effects

of strong electron correlations. At $x > 0.5$, some of the Co states may be localised by these interactions causing the Curie-Weiss-like magnetic behaviour and spin wave excitations, whilst the material retains metallic conductivity. Below half doping the electron correlation effects are weaker and the system is Pauli paramagnetic. Therefore there must exist a cross-over between these two regimes, a special state realised at $x = 0.5$ in which the magnetism is largely described by the itinerant electron picture but electron correlation effects play a role in the formation of the MIT. It should be noted that the insulating transition is anisotropic; the resistivity at low temperatures along c is $25 \Omega\text{cm}$ and just $15 \text{ m}\Omega\text{cm}$ along ab ¹⁴, a value comparable to that of the “metallic” SDW system⁸, and whilst $\text{Na}_{\frac{1}{2}}\text{CoO}_2$ is considered a low temperature insulator in dc, optical conductivity measurements¹⁵ reveal the MIT is only visible in the low frequency data. The mechanism that drives the MIT is clearly not yet understood and further investigation into the electronic band structure at this doping level is needed.

In summary, the intraplanar magnetic excitations whose zone centres coexist with structural Bragg reflections have been studied. The excitation has a gap of $11.5(5)$ meV. The localized spin model does not provide physically realistic values for the magnon velocity or the energy transfer at the zone boundary and is not consistent with the broadening and diminishing scattering more reminiscent to the transformation between spin wave and Stoner excitations as seen in the itinerant magnets. The excitation modes measured in this study indicate that the system is at least partially itinerant and that a model containing zero spin Co^{3+} and spin-half Co^{4+} is not appropriate.

We thank Julie Staunton and Jim Hague for insightful discussions and acknowledge financial support from the EPSRC. Both neutron scattering experiments were funded within the EU NMI3 access program.

¹ K. Takada, H. Sakurai, E. Takayama-Muromachi, F. Izumi, R. A. Dilanian, and T. Sasaki, *Nature* **422**, 53 (2003).
² L. M. Helme, A. T. Boothroyd, R. Coldea, D. Prabhakaran, D. A. Tennant, A. Hiess, and J. Kulda, *Phys. Rev. Lett.* **94**, 157206 (2005).
³ S. P. Bayrakci, I. Mirebeau, P. Bourges, Y. Sidis, M. Endterle, J. Mesot, D. P. Chen, C. T. Lin, and B. Keimer, *Phys. Rev. Lett.* **94**, 157205 (2005).
⁴ G. Gašparović, R. A. Ott, J.-H. Cho, F. C. Chou, Y. Chu, J. W. Lynn, and Y. S. Lee, *Phys. Rev. Lett.* **96**, 046403 (2006).
⁵ Q. Huang, M. L. Foo, J. W. Lynn, H. W. Zandbergen, G. Lawes, Y. Wang, B. H. Toby, A. P. Ramirez, N. P. Ong, and R. J. Cava, *J. Phys.: Condens. Matter* **16**, 5803 (2004).
⁶ J. Bobroff, G. Lang, H. Alloul, N. Blanchard, and G. Collin, *Phys. Rev. Lett.* **96**, 107201 (2006).
⁷ A. J. Williams, J. P. Attfield, M. L. Foo, and R. J. Cava, *Phys. Rev. B* **73**, 134401 (2006).
⁸ J. Wooldridge, D. M. Paul, G. Balakrishnan, and M. R. Lees, *J. Phys.: Condens. Matter* **17**, 707 (2005).
⁹ T. P. Choy, D. Galanakis, and P. Phillips (2006), cond-mat/0502164.
¹⁰ A. T. Boothroyd, R. Coldea, D. A. Tennant, D. Prabhakaran, L. M. Helme, and C. D. Frost, *Phys. Rev. Lett.* **92**, 197201 (2004).
¹¹ M. D. Johannes, I. I. Mazin, and D. J. Singh, *Phys. Rev. B* **71**, 214410 (2005).
¹² S. K. Burke, W. G. Stirling, K. R. A. Ziebeck, and J. G. Booth, *Phys. Rev. Lett.* **51**, 494 (1983).
¹³ S. Tomiyoshi, Y. Yamaguchi, M. Ohashi, E. R. Cowley, and G. Shirane, *Phys. Rev. B* **36**, 2181 (1987).
¹⁴ C. H. Wang, X. H. Chen, J. L. Luo, G. T. Liu, X. X. Lu, H. T. Zhang, G. Y. Wang, X. G. Luo, and N. L. Wang, *Phys. Rev. B* **71**, 224515 (2005).
¹⁵ N. L. Wang, D. Wu, G. Li, X. H. Chen, C. H. Wang, and X. G. Luo, *Phys. Rev. Lett.* **93**, 147403 (2004).